Momentum-resolved spectral functions of $SrVO_3$ calculated by LDA+DMFT

I. A. Nekrasov,[1,2] K. Held,[3] G. Keller,[2] D. E. Kondakov,[4] Th. Pruschke,[5] M. Kollar,[2] O. K. Andersen,[3] V. I. Anisimov,[4] and D. Vollhardt[2]

[1]*Institute for Electrophysics, Russian Academy of Sciences, Ekaterinburg 620016, Russia*

[2]*Theoretical Physics III, Centre for Electronic Correlations and Magnetism, University of Augsburg, 86135 Augsburg, Germany*

[3]*Max-Planck Institute for Solid State Research, Heisenbergstrasse 1, 70569 Stuttgart, Germany*

[4]*Institute of Metal Physics, Russian Academy of Sciences, Ekaterinburg 620219, Russia*

[5]*Institute for Theoretical Physics, University of Göttingen, Tammannstrasse 1, 37077 Göttingen, Germany*

(Received 12 August 2005; revised manuscript received 12 December 2005; published 18 April 2006)

LDA+DMFT, the merger of density functional theory in the local density approximation and dynamical mean-field theory, has been mostly employed to calculate $\boldsymbol{k}$-integrated spectra accessible by photoemission spectroscopy. In this paper, we calculate $\boldsymbol{k}$-*resolved* spectral functions by LDA+DMFT. To this end, we employ the *N*th order muffin-tin (NMTO) downfolding to set up an effective low-energy Hamiltonian with three t_{2g} orbitals. This downfolded Hamiltonian is solved by DMFT yielding $\boldsymbol{k}$-dependent spectra. Our results show a renormalized quasiparticle band over a broad energy range from −0.7 eV to +0.9 eV with small "kinks" discernible in the dispersion below the Fermi energy.

DOI: 10.1103/PhysRevB.73.155112 PACS number(s): 71.27.+a, 71.30.+h, 71.15.Mb

I. INTRODUCTION

Transition metal oxides show a diversity of challenging physical phenomena, including superconductivity, metal-insulator transitions, and colossal magnetoresistance, and are therefore at the center of modern solid state research. Electrons in many of these materials are strongly correlated due to a large ratio of Coulomb interaction to bandwidth U/W, resulting in complicated many-electron physics which makes realistic calculations rather difficult. In particular, conventional band structure calculations, e.g., in the local density approximation (LDA),[1] fail because these effective one-particle approaches do not contain many-body physics such as the formation of Hubbard bands, quasiparticle renormalization, and lifetime effects. In this respect LDA+DMFT, the recent merger[2–7] of LDA with the many-body dynamical mean-field theory (DMFT),[8–11] is a promising new approach which includes many-body aspects into realistic calculations. It has been successfully applied, in particular to calculate the total ($\boldsymbol{k}$-integrated) spectra of transition-metal oxides like $LaTiO_3$,[2,12] V_2O_3,[13–15] $Sr(Ca)VO_3$,[15,17–22] LiV_2O_4,[23] $Ca_{2-x}Sr_xRuO_4$,[24,25] CrO_2,[26] but also of Ni,[27] Fe,[27] and *f*-electron systems such as Pu[28,29] and Ce.[30–35]

LDA+DMFT calculations for transition metal oxides have mostly been restricted to the *d* bands around the Fermi energy, employing a simplified calculational scheme based on the LDA density of states (DOS) which holds for cubic systems.[3] Calculations with the full LDA Hamiltonian, including all *spdf* valence orbitals in the DMFT have been performed for Pu[28,29] and Ce.[30–33] Since the O_{2p}-Me_{3d} overlap is considerable for transition metal (TM) oxides, a full LDA Hamiltonian calculation should also take into account the rather large[36–38] oxygen-TM and oxygen-oxygen Coulomb interactions U_{pd} and U_p.

While a large number of interacting orbitals makes LDA+DMFT calculations with the full *spd* Hamiltonian difficult, they are feasible for the effective *d* bands around the Fermi energy. To this end, a clear definition of the effective Hamiltonian for energies near the Fermi energy is mandatory. An accurate construction of this effective Hamiltonian is possible by the downfolding procedure for third generation muffin-tin orbitals[39] (NMTOs) and has recently been employed in the LDA+DMFT context by Pavarini *et al.*[19,22] Furthermore, Anisimov *et al.*[15] recently proposed a projection scheme of the Bloch functions onto a Wannier functions basis to obtain a few-orbital Hamiltonian. Also note a third scheme, proposed by Solovyev,[16] for generating Wannier functions from LMTO Bloch functions. Such a downfolded or projected Hamiltonian is required to calculate $\boldsymbol{k}$-resolved spectra.

Due to its simple crystal structure (cubic perovskite) and the $3d^1$ electronic configuration the transition metal oxide $SrVO_3$ is ideal for testing new theoretical methods for the realistic modeling of correlated materials. $SrVO_3$ is a strongly correlated metal with a pronounced lower Hubbard and quasiparticle peak in the photoemission spectra[40–42] (PES) as well as a pronounced quasiparticle and upper Hubbard band in the x-ray absorption spectrum.[43] After the substitution of Sr by Ca, PES[40] and Bremsstrahlung isochromat spectra[44] (BIS) originally suggested the onset of a Mott-Hubbard metal-insulator transition. By contrast, thermodynamic properties (Sommerfeld coefficient, resistivity, and paramagnetic susceptibility)[45] did not show significant effects upon Ca doping. An attempt to describe electronic properties of $SrVO_3$ by DMFT was made by Rozenberg *et al.*[46,47] for the one-band Hubbard model using phenomenological parameters. Recently, the puzzling discrepancy between spectroscopic and thermal properties has been solved by new bulk-sensitive PES,[41,42,48] showing similar spectra for $CaVO_3$ and $SrVO_3$, in agreement with the thermodynamic results. This was confirmed theoretically by LDA+DMFT calculations.[15,18–22] In this paper we present LDA+DMFT (QMC) calculations for $SrVO_3$ based on a NMTO downfolded effective Hamiltonian for three orbitals of t_{2g}

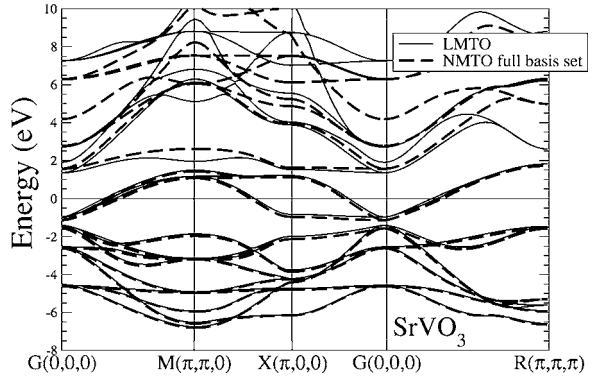

FIG. 1. Comparison of the LDA band structure of $SrVO_3$ calculated by LMTO (thin solid line) and NMTO (dashed line) for the full orbital basis set. Here, and in the following figures, the Fermi energy corresponds to zero energy.

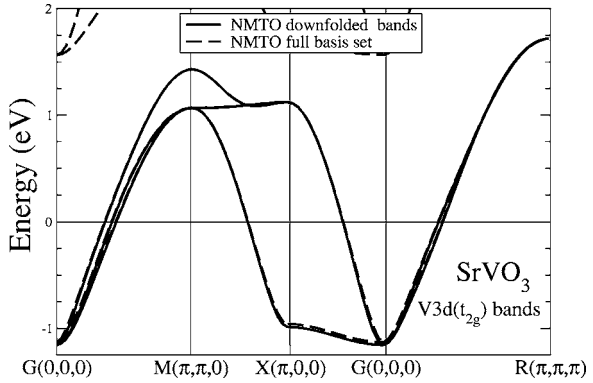

FIG. 2. Comparison of the NMTO downfolded t_{2g} bands (full line) with NMTO for the full orbital basis set (dashed line).

symmetry crossing the Fermi energy. From this we calculate $\boldsymbol{k}$-resolved spectral functions and ARPES spectra. Recently angular-resolved photoemission spectroscopy (ARPES) on $SrVO_3$ was performed;[48,49] the data from Fujimori's group[49] allow for the direct observation of the quasiparticle mass renormalization and band edge.

The paper is organized as follows. In Sec. II we briefly discuss the crystal structure and calculate the effective t_{2g} Hamiltonian for $SrVO_3$ by LDA/NMTO. In Sec. III, we discuss and compare two LDA+DMFT (QMC) calculations for $SrVO_3$, based on this effective t_{2g} Hamiltonian and a simplified treatment using the DOS only. Finally, in Sec. IV the LDA+DMFT (QMC) calculated self-energy on the real axis $\Sigma(\omega)$ and $\boldsymbol{k}$-resolved spectral functions for $SrVO_3$ are presented. The paper is summarized in Sec. V.

II. CONSTRUCTION OF FEW-ORBITAL HAMILTONIANS

Starting point of a first principle calculation is usually the crystal structure. In our case, $SrVO_3$ is a perovskite with an ideal cubic $Pm\bar{3}m$[50] symmetry, containing one V ion in the unit cell. This implies that the main structural element, the VO_6 octahedron, is not distorted. The electronic configuration is $3d^1$, which follows from the formal oxidation V^{4+}. Due to the cubic symmetry, the d orbitals split into two sets: three t_{2g} and two e_g orbitals. In our case of an octahedral coordination with oxygen, the threefold degenerated t_{2g} orbitals are lower in energy than the twofold e_g orbitals. Since these t_{2g} and e_g bands do not overlap we will later restrict our calculation to an effective Hamiltonian with three t_{2g} orbitals filled with one electron per site.

For the LDA band structure calculations of $SrVO_3$ we first employed the LDA-LMTO (ASA) code version 47 which uses the basis of nonorthogonal linearized muffin-tin orbitals (LMTO; 2nd generation) in the atomic sphere approximation (ASA).[51] Thereby, the partial waves were expanded to linear order in energy around the center of gravity of the filled part of the bands. The results are presented by thin solid lines in Fig. 1 and show $2p$ oxygen bands below -1.5 eV, three t_{2g} bands at the Fermi energy between -1.5 eV and 1.5 eV, and e_g bands between 1.5 eV and 6 eV. The other bands of our orbital basis set $[\mathrm{O}(3s,3d),\ \mathrm{V}(4s,4p),\ \mathrm{Sr}(5s,5p,4d,4f)]$ are empty and lie far above the Fermi level.[52]

Second, with the same basis set we employed the third generation MTO, also known as Nth order muffin tin orbitals (NMTO).[39] We expanded the MTOs around the three points: -2.72 eV, 0.68 eV, and 6.8 eV. Here and in the following, all energies are measured relative to the Fermi energy at 0 eV. The NMTO results are shown as dashed lines in Fig. 1 and almost coincide with LMTOs in the region of interest, i.e., O $2p$ and V $3d$. The NMTO bands are found to be slightly lower in energy which is not surprising since third generation MTOs have the proper energy dependence in the interstitial region and, moreover, more expansion points ($N+1=4$) for the wave function than LMTOs where $N=1$ (linear approach). For the high-lying empty bands, LMTO and NMTO bands are quite different; the NMTO bands are again lower in energy. As the third NMTO expansion point (6.8 eV) is in this region, we expect NMTOs to be more precise in this region than LMTOs, which are linearized at energies corresponding to the center of gravity of the *filled* parts of the bands. Hence, the LMTO expansion points are below the Fermi energy, far away from these high-lying empty bands. Moreover, the second generation LMTOs have vanishing kinetic energy in the interstitial region.

A particular advantage of NMTOs is the possibility of calculating an effective (downfolded) Hamiltonian $\hat{H}^{\mathrm{eff}}(\boldsymbol{k})$, confined to a reduced set of orbitals in a reduced window of energies. In the case of $SrVO_3$, the t_{2g} subset of the V $3d$ orbitals is of particular interest as discussed above. Hence, we downfolded[39] to a 3×3 NMTO Hamiltonian $\hat{H}^{\mathrm{eff}}(\boldsymbol{k})$ describing the three t_{2g} orbitals. For optimizing the energy window with respect to these orbitals, we chose two MTO expansion points, $\epsilon_0=0.41$ eV and $\epsilon_1=0.95$ eV, at the energy region of the t_{2g} bands. At these energies, the NMTOs span exactly the LDA eigenfunctions. Figure 2 shows the eigenvalues of $\hat{H}^{\mathrm{eff}}(\boldsymbol{k})$ along some high-symmetry directions in comparison with the NMTO results using the full orbital basis of Fig. 1. From the good agreement we conclude that $\hat{H}^{\mathrm{eff}}(\boldsymbol{k})$ describes the three t_{2g} bands well. The slight discrepancy at the bottom of the band could have been avoided by choosing a smaller value of ϵ_0. If we increase the number of these mesh points ϵ_i, the Hilbert space spanned by these

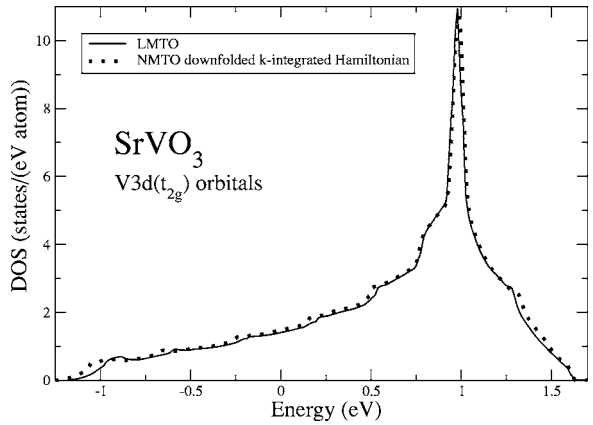

FIG. 3. Comparison of the t_{2g} DOS calculated (i) by LMTO as explained in the text (thin solid line) and (ii) by integrating the down-folded NMTO Hamiltonian over the Brillouin zone (dotted line).

NMTOs will converge to that spanned by the t_{2g} Wannier functions; the orthogonalization of these NMTOs will yield localized Wannier functions.

Figure 3 compares the DOS of $\hat{H}^{\text{eff}}(\boldsymbol{k})$ obtained via tetrahedron integration[53] with the LMTO DOS. A minor difference to earlier calculations[18,21] is that we used an orthogonal representation of the LMTO method in Refs. 18 and 21, neglecting the so-called combined correction term. Because of this Refs. 18 and 21 yield a slightly different t_{2g} band shape with a discernible reduction of the sharp peak at ≈ 1 eV. These differences are, however, small and unimportant for the final LDA+DMFT results. For the LMTO DOS of Fig. 3, we downfolded the band structure onto the t_{2g} states which, due to the oxygen $2p$-t_{2g} hybridization, also have a contribution between -7 eV and -2 eV. Vice versa, downfolding to O-$2p$ states gives a contribution around the Fermi energy. To obtain the *effective* t_{2g} orbitals at the Fermi energy (which have primarily t_{2g} character with a small $2p$ admixture) we truncated the t_{2g} contribution in the oxygen region between -7 eV and -2 eV and renormalized the orbitals so that one has again one electron per site and orbital. Figure 3 shows that the DOS calculated by this procedure resembles the downfolded NMTO DOS well. In particular, both DOSs have the same features and bandwidth. The agreement with the NMTO DOS of Ref. 19 is also very good.

III. LDA+DMFT CALCULATIONS USING DOWNFOLDING AND HILBERT TRANSFORM

In this section, we will use two different methods to construct the noninteracting, i.e., kinetic energy part, of the three-band many-body problem: the NMTO downfolded t_{2g} Hamiltonian $\hat{H}^{\text{eff}}(\boldsymbol{k})$ and the LMTO DOS of Fig. 3. This part of the Hamiltonian is then complemented by a local Coulomb interaction

$$\hat{H} = \hat{H}_0^{\text{eff}} + U \sum_m \sum_i \hat{n}_{im\uparrow}\hat{n}_{im\downarrow} + \sum_i \sum_{m\neq m'} \sum_{\sigma\sigma'} (U' - \delta_{\sigma\sigma'}J)\hat{n}_{im\sigma}\hat{n}_{im'\sigma'}. \quad (1)$$

Here, the index i enumerates correlated lattice sites, m denotes orbitals, and σ the spin. $\hat{H}_0^{\text{eff}}$ is a one-particle Hamiltonian generated from the LDA band structure where an averaged Coulomb interaction is subtracted to avoid double counting of the Coulomb interaction.[2,3] The local intraorbital Coulomb repulsion is denoted by U and the Hund's exchange coupling by J. Rotational invariance then fixes the local interorbital Coulomb repulsion $U' = U - 2J$, see, e.g., Ref. 54. For three orbitals, U' equals the averaged Coulomb interaction $\bar{U}$.[3,12]

The Hamiltonian (1) is then solved by the recently developed LDA+DMFT approach[2] (for introductions see Refs. 3 and 6, for reviews see Refs. 4, 5, and 7). In this approach the solution of (1) is obtained by the dynamical mean-field theory (DMFT),[9–11] a nonperturbative many-body method based on the $d=\infty$ limit.[8]

In this paper, $\hat{H}_0^{\text{eff}}$ will be the NMTO downfolded (and symmetrically orthonormalized) Hamiltonian of Sec. II. The double counting correction is not relevant here since we consider only the three correlated t_{2g} orbitals.[3,12] To calculate Coulomb interaction parameters appearing in (1) we previously[18,21] employed the constrained LDA method,[55] yielding an orbitally averaged Coulomb repulsion $\bar{U}=3.55$ eV and a Hund's exchange coupling $J=1.0$ eV.

In our LDA+DMFT calculations, we self-consistently solve the auxiliary DMFT impurity problem[9–11] by multiband quantum Monte Carlo (QMC) simulations[56] together with the $\boldsymbol{k}$-integrated Dyson equation

$$\boldsymbol{G}(\omega) = \int_{\text{BZ}} d\boldsymbol{k}[\omega + \mu - \boldsymbol{\Sigma}(\omega) - \boldsymbol{h}_0^{\text{eff}}(\boldsymbol{k})]^{-1}. \quad (2)$$

Here, $\boldsymbol{G}(\omega)$, $\boldsymbol{\Sigma}(\omega)$, and $\boldsymbol{h}_0^{\text{eff}}(\boldsymbol{k})$ are 3×3 matrices in orbital space, denoting the Green function, self-energy, and the downfolded NMTO Hamiltonian $\hat{H}_0^{\text{eff}}$ in reciprocal space, respectively; μ is the chemical potential. The simulations were done for an inverse temperature $\beta=10$ eV^{-1}, using 40 imaginary time slices ($\Delta\tau=0.25$) and 2×10^6 Monte Carlo sweeps. Since QMC is formulated on the imaginary axis, we employed Eq. (2) for Matsubara frequencies and analytically continued $G(i\omega)$ to real frequencies by means of the maximum entropy method.[57] We checked the accuracy of the calculated maximum entropy method (MEM) spectral density $A(\omega)$ by performing ten independent self-consistent DMFT (QMC) runs, at given $\hat{H}_0^{\text{eff}}$ and QMC parameters. The accuracy of the chemical potential is 0.005 eV; in the relevant energy range ± 0.5 eV around the Fermi energy, the MEM accuracy is 0.05 eV in ω and 2% in amplitude for $A(\omega)$. Further away from the Fermi energy, the MEM accuracy decreases. In our previous calculations,[18,21] we used a simplified scheme based on the LDA DOS only. Within a cubic symmetry, the local DMFT self-energy becomes diagonal and even orbital independent: $\Sigma_{mm'\sigma\sigma'}(\omega) = \delta_{mm'}\delta_{\sigma\sigma'}\Sigma(\omega)$. Then, the Green functions $G(\omega)$ of the lattice problem can be expressed via the Hilbert transform of the LDA DOS $N^0(\epsilon)$

$$G(\omega) = \int d\epsilon \frac{N^0(\epsilon)}{\omega + \mu - \epsilon - \Sigma(\omega) + i\eta}, \quad (3)$$

instead of Eq. (2).

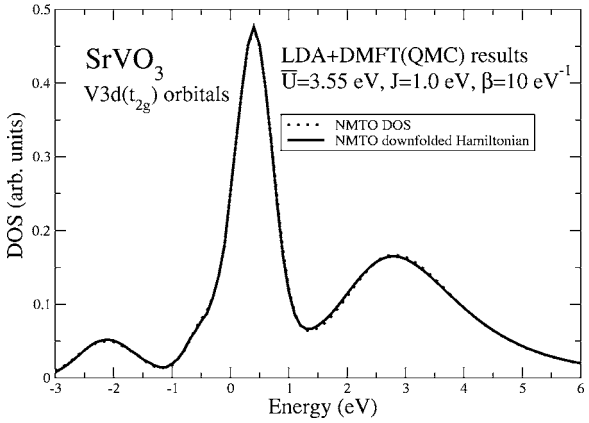

FIG. 4. Comparison of the LDA+DMFT (QMC) $\boldsymbol{k}$-integrated $SrVO_3$ spectrum of the three t_{2g} bands crossing the Fermi energy obtained by NMTO (dotted line) and by the NMTO downfolded t_{2g} Hamiltonian (full line), respectively. The local Coulomb interaction was calculated by constrained LDA as $\bar{U}=3.55$ eV and $J=1.0$ eV; the temperature is 0.1 eV.

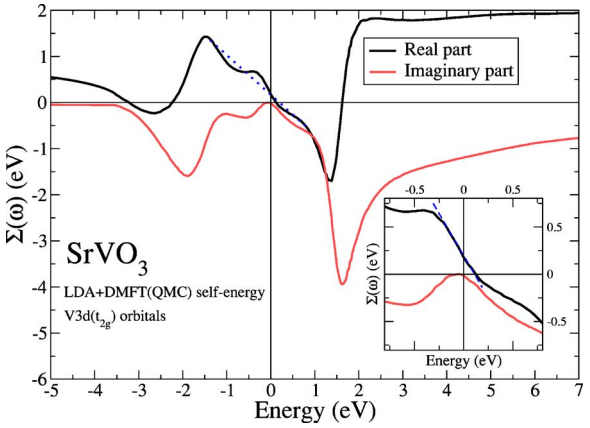

FIG. 5. (Color online) Real [black line] and imaginary [red (gray) line] parts of the LDA+DMFT(QMC) self-energy $\Sigma(\omega)$ for the vanadium t_{2g} orbitals of $SrVO_3$ (see text). The inset shows the magnification of $\mathrm{Re}\,\Sigma(\omega)$ and $\mathrm{Im}\,\Sigma(\omega)$ near the Fermi level. The dotted line in the main panel indicates the linearization for the whole range of the central peak (−0.8 to 1.4 eV; main figure), while the dashed line in the inset marks the strict quasiparticle regime from −0.2 eV to +0.15 eV.

In Fig. 4, we present a comparison between one-particle LDA+DMFT (QMC) spectra for $SrVO_3$ obtained by using Eq. (3) with the Vanadium t_{2g} LDA DOS (thin solid line in Fig. 3; calculated as described in Sec. II) and Eq. (2) with $\boldsymbol{h}_0^{\mathrm{eff}}(\boldsymbol{k})$. Both methods give the same results, as is to be expected for a cubic system. One can see the generic "three-peak" spectrum of a strongly correlated metal: the quasiparticle peak slightly above the Fermi energy, and lower and upper Hubbard bands to the left and right. The results presented here agree well with those reported in Refs. 15 and 18–22. The LDA+DMFT calculations of Ref. 17, with a focus on bulk surface differences, used a somewhat lower Coulomb interaction $\bar{U}=U-2J=2.6, 2.9$ eV.

IV. CALCULATION OF k-RESOLVED SPECTRA

The purpose of this paper is to calculate the $\boldsymbol{k}$-resolved spectral function $A(\boldsymbol{k},\omega)$ for $SrVO_3$ within the LDA+DMFT(QMC) scheme. Here

$$A(\boldsymbol{k},\omega) = -\frac{1}{\pi}\,\mathrm{Im\,Tr}\,\boldsymbol{G}(\boldsymbol{k},\omega) \tag{4}$$

is determined by the diagonal elements of the Green function matrix in orbital space

$$\boldsymbol{G}(\boldsymbol{k},\omega) = [\omega - \boldsymbol{\Sigma}(\omega) - \boldsymbol{h}_0^{\mathrm{eff}}(\boldsymbol{k})]^{-1}. \tag{5}$$

From this definition one can see that the two necessary ingredients to calculate $A(\boldsymbol{k},\omega)$ are (i) the Hamiltonian matrix $\boldsymbol{h}_0^{\mathrm{eff}}(\boldsymbol{k})$, and (ii) the self-energy matrix $\boldsymbol{\Sigma}(\omega)$ at real frequencies. Similar schemes were recently used by Liebsch and Lichtenstein[24] to compute quasiparticle properties of Sr_2RuO_4 and by Biermann *et al.* to describe the presence of a lower Hubbard band in γ-Mn.[58] Angle-resolved photoemission spectra of the two-dimensional (2D) Hubbard model were also investigated by Maier *et al.*[59] in the framework of the dynamical cluster approximation[60] (DCA) and by Sadovskii *et al.*[61] within the so-called DMFT+Σ_k approach. Within DMFT the self-energy on the real axis was also calculated in Refs. 15 and 62.

In our case of cubic symmetry, $\Sigma(\omega)$ is the same for all t_{2g} orbitals. Eqs. (2) and (5) are formulated in terms of a self-energy $\Sigma(\omega)$ for *real* frequencies ω. Since LDA+DMFT (QMC) determines the self-energy $\Sigma(i\omega_n)$ for Matsubara frequencies $i\omega_n$, the calculation of $\Sigma(\omega)$ requires a separate calculation. To this end we first employ the maximum entropy method[57] to obtain the $\boldsymbol{k}$-integrated, spectral function $A(\omega) = -\frac{1}{\pi}\,\mathrm{Im}\,G(\omega)$ with $G(\omega) \equiv [\boldsymbol{G}(\omega)]_{mm}$, shown in Fig. 4. The Kramers-Kronig relation

$$\mathrm{Re}\,G(\omega) = -\frac{1}{\pi}\int_{-\infty}^{\infty} d\omega' \frac{\mathrm{Im}\,G(\omega')}{\omega - \omega' + i\eta} \tag{6}$$

then determines the real part of the Green function. The complex Green function and the complex self-energy are related by the $\boldsymbol{k}$-integrated Dyson Eq. (2). We obtain the self-energy as the numerical solution of Eq. (2).

The unknown complex self-energy enters in the integrand of Eq. (2). After rewriting Eq. (2) as a system of two equations for the real (Re) and imaginary (Im) part of the Green function $G(\omega)$ we solved the two equations iteratively for each energy ω. The convergence criterion was chosen as $|\mathrm{Re}\,\Sigma_i(\omega) - \mathrm{Re}\,\Sigma_{i-1}(\omega)| + |\mathrm{Im}\,\Sigma_i(\omega) - \mathrm{Im}\,\Sigma_{i-1}(\omega)| < \epsilon$, where i denotes the iteration. The accuracy of the converged solution was $\epsilon=0.001$ eV for all energy points (also see Ref. 15 Appendix B).

Figure 5 presents the resulting real and imaginary parts of the self-energy $\Sigma(\omega)$ as a function of real frequencies ω. The calculated self-energy satisfies the Kramers-Kronig relation

$$\mathrm{Re}\,\Sigma(\omega) = -\frac{1}{\pi}\int_{-\infty}^{\infty} d\omega' \frac{\mathrm{Im}\,\Sigma(\omega)}{\omega - \omega'} + \mathrm{cons}. \tag{7}$$

The self-energy is highly asymmetric with respect to the Fermi level, as expected for the present case of an asymmetric LDA DOS and 1/6 band filling. At the energies $\omega \sim \pm 1.5$ eV the real part of the self-energy, $\mathrm{Re}\,\Sigma$, has extrema, originating from the crossover from the central quasiparticle peak to the lower and upper Hubbard bands. The two extrema of $\mathrm{Im}\,\Sigma$, which coincide with zeros of $\mathrm{Re}\,\Sigma$, are responsible for the strong incoherence of the lower and upper Hubbard bands (see Fig. 4).

Let us now turn from the Hubbard bands to the energy regime of the central (quasiparticle) peak, ranging from about −0.8 eV to 1.4 eV in Fig. 4. The imaginary part of the self-energy $\mathrm{Im}\,\Sigma(\omega)$ is still relatively small in this regime and the real part of the self-energy can roughly be described by a straight line (dashed line in Fig. 5, main panel). This line corresponds to a quasiparticle weight $Z=m^\star/m=1-\partial\,\mathrm{Re}\,\Sigma(\omega)/\partial\omega|_{\omega=0}=1.9$, describing the reduction of the quasiparticle bandwidth from approximately 3 eV in LDA to 1.5 eV in LDA+DMFT. This value for $m^\star/m$ is in accord with the one determined from the lowest Matsubara frequency ω_0, i.e., $m^\star/m=1-[\mathrm{Im}\,\Sigma(\omega_0)/\omega_0]\approx 2$, and the estimate from the overall weight of the central (quasiparticle) peak (from −0.8 eV to 1.4 eV: $1/Z=m^\star/m\approx 2.2$). It is also close to the value $m^*/m=2.2$ calculated in Refs. 19 and 22 and the value $m^*/m=1.8\pm 0.2$ obtained in recent ARPES experiments.[49] However, the inset of Fig. 5 reveals that, strictly speaking, the Fermi liquid regime with $\mathrm{Im}\,\Sigma(\omega)\sim-\omega^2$ and $\mathrm{Re}\,\Sigma(\omega)\sim-\omega$ only extends from −0.2 up to 0.15 eV. In this energy range the slope of $\mathrm{Re}\,\Sigma(\omega)$ (indicated by a dashed line) is steeper than the slope of the dotted line shown in the main panel of Fig. 5. The effective mass in this low-energy regime is $m^*_{\mathrm{low}E}/m=3$. This is somewhat larger than the overall mass renormalization $m^*/m=1.9$ describing the reduction in bandwidth.

Next to this Fermi liquid regime, there are pronounced shoulders in $\mathrm{Re}\,\Sigma(\omega)$ at $\omega=-0.25$ eV and +0.25 eV, with corresponding "kink"-like structures in $\mathrm{Im}\,\Sigma(\omega)$, according to the Kramers-Kronig relation (7). These shoulders of $\mathrm{Re}\,\Sigma(\omega)$ will become important in the context of the quasiparticle dispersion in Fig. 8.

Remarkably, similar "kink"-like structures on the scale of 0.1 eV below the Fermi energy were recently observed in ARPES experiment on $SrVO_3$ by Yoshida *et al.*[49] Also note that similar structures for $\mathrm{Im}\,\Sigma(\omega)$ can be found in Ref. 62, based on LDA+DMFT (QMC) calculations for $LaTiO_3$.[12] Because of the above-mentioned shoulders in $\mathrm{Re}\,\Sigma(\omega)$, $\mathrm{Re}\,\Sigma(\omega)$ can be roughly approximated by a straight line (dashed line of the main panel Fig. 5) in the overall energy regime of the central quasiparticle peak.

With the knowledge of the self-energy on the real axis, we are now in the position to calculate the $\boldsymbol{k}$-resolved spectral functions Eqs. (4) and (5) and the quasiparticle dispersion. In Fig. 6, the LDA+DMFT (QMC) spectral functions $A(\boldsymbol{k},\omega)$ for $SrVO_3$ are presented. In the energy regions [−3 eV, −1 eV] and [1.5 eV, 5 eV] there is some broad, nondispersive spectral weight corresponding to the incoherent lower and upper Hubbard bands, which are hardly visible due to their almost homogeneous distribution over the whole of the Brillouin zone. Around the Fermi energy, $A(\boldsymbol{k},\omega)$ shows a dispersive peak which is somewhat smeared out away from the Fermi energy because of lifetime effects, $\tau^{-1}\sim\omega^2$; Fig. 7 shows a magnification in the vicinity of the Fermi energy.

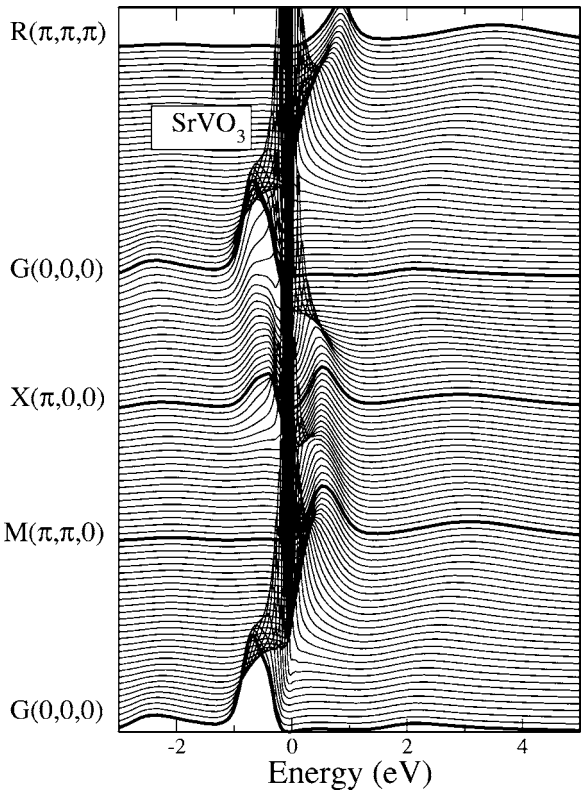

FIG. 6. Spectral function $A(\boldsymbol{k},\omega)$ for the three V-3$d(t_{2g})$ bands of $SrVO_3$ as calculated by LDA+DMFT(QMC); for the behavior around the Fermi energy see Fig. 7.

The $\boldsymbol{k}$-resolved spectral functions in turn allow us to determine the LDA+DMFT (QMC) quasiparticle band, which are shown as dots in Fig. 8 and compared to the bare LDA bands (solid lines). These dots are the maxima of the spectral function from Figs. 6 and 7 around the Fermi level where the quasiparticles are well defined. They resemble the LDA dispersion, albeit renormalized. This is to be expected for a Fermi liquid, where

$$\boldsymbol{G}(\omega)=Z\int_{\mathrm{BZ}} d\boldsymbol{k}[\omega+Z\mu-Z\boldsymbol{h}_0^{\mathrm{eff}}(\boldsymbol{k})]^{-1} \tag{8}$$

in the quasiparticle region. Employing this Fermi liquid behavior, and using $1/Z=1.9$, we can reconstruct the band structure directly from the LDA spectrum. As seen from Fig. 8, the result (dashed curves) agrees well with the quasiparticle band (dots). However it should be noted that changes in slope of the LDA+DMFT (QMC) dispersion occur at $\omega=-0.25$ eV and (hardly discernible) $\omega=+0.25$ eV (see Fig. 8). These kinks[63,64] stem from the shoulders in the real part of the self-energy (Fig. 5) and occur when the effective dispersion crosses over from the Fermi liquid regime with $m^\star_{\mathrm{low}E}/m\approx 3$ to the LDA band structure with constant renormalization $m^\star/m\approx 1.9$. Similar "kink"-like structures were recently found by us in DMFT calculations for the one-band Hubbard model off half filling, with the numerical renormal-

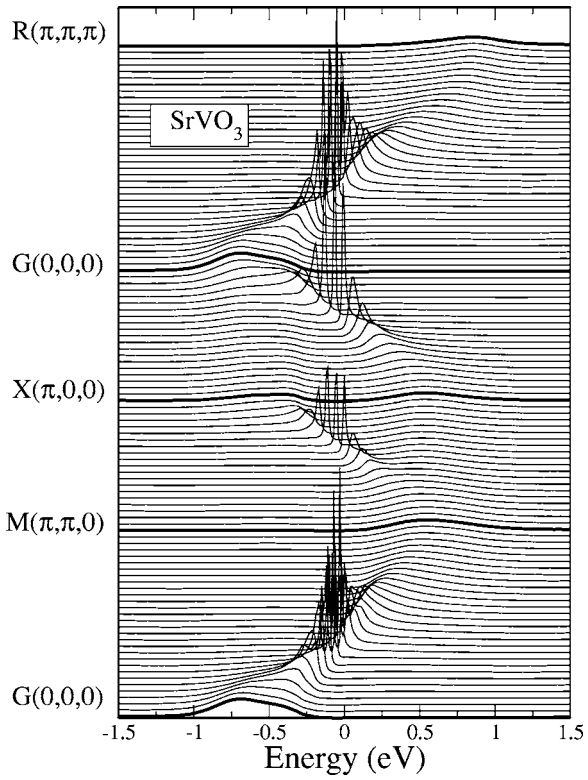

FIG. 7. Magnification of Fig. 6 around the Fermi energy (0 eV); the ARPES amplitude is five times smaller than in Fig. 6.

ization group used as an impurity solver. Presumably these kinks reflect interactions between correlated electrons and local charge/spin fluctuations. The particular contribution of each type of fluctuation at this energy interval is presently under investigation. Strong interest in kinks of the dispersion has followed their observation in various high-T_c superconductors,[65] where they have been attributed mainly to phonons. In electronic systems kinks in the dispersion have also been found in theoretical studies of the 2D Hubbard model within the fluctuation exchange approximation[66] and most recently within the self-consistent projection operator method.[67]

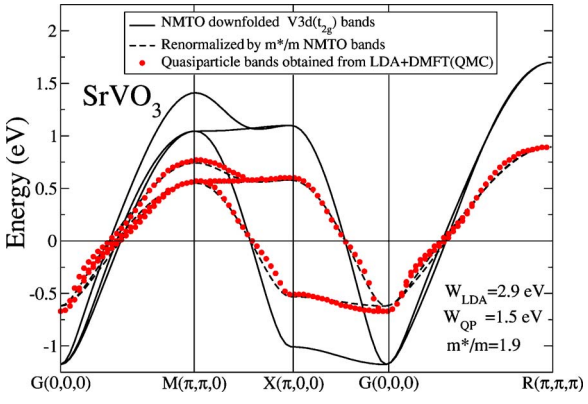

FIG. 8. (Color online) LDA+DMFT(QMC) dispersion for $SrVO_3$ (dots) compared with LMTO (full line) and quasiparticle renormalization of the LMTO dispersion by $Z=1/1.9$ (dashed line). The ratio of bandwidths yields $1/Z=m^\star/m=1.9$. The dashed line represents a simple quasiparticle renormalization of the NMTO bands by $1/Z=1.9$. At $\omega=-0.25$ eV, we see a kink in the LDA+DMFT(QMC) dispersion (dots), clearly discernible as a deviation from the simple renormalized LDA bands (dashed line).

When comparing with experiments, we note that for ***k**-resolved* spectra the influence of PES matrix elements may be stronger than for the ***k***-integrated spectra. Nevertheless, their inclusion affects the relative intensities but not their position. We find qualitative agreement with recent ARPES dispersions,[49] where the renormalized band structure was observed directly. In particular, we see from Fig. 8 that the bottom of the quasiparticle band is located at approximately $\omega=-0.7$ eV, in contrast to the LDA value of $\omega=-1.2$ eV.

V. CONCLUSION

In this paper, we presented LDA+DMFT (QMC) computations of ***k***-resolved spectral functions of $SrVO_3$. The necessary input is an LDA-calculated Hamiltonian $\hat{H}_0^{\text{eff}}$ and the LDA+DMFT self-energy at real frequencies $\Sigma(\omega)$. We used the NMTO downfolding to calculate $\hat{H}_0^{\text{eff}}$ for the strongly correlated V-$3d(t_{2g})$ orbitals of $SrVO_3$ crossing the Fermi energy. This calculation gives essentially the same ***k***-integrated spectrum as our previous calculations[18,21] based on the t_{2g} projected DOS.

The LDA+DMFT ***k***-resolved spectral function $A(\boldsymbol{k},\omega)$ shows two incoherent Hubbard bands and a dispersive quasiparticle band. The latter is determined from the maxima of $A(\boldsymbol{k},\omega)$ and resembles the LDA dispersion renormalized by a constant factor $m^\star/m=1.9$. This effective mass renormalization describes the *overall* reduction of the quasiparticle bandwidth from approximately 3 eV in LDA to 1.5 eV in LDA+DMFT, and agrees with the mass renormalization found in ARPES experiments.[49] However, close to the Fermi surface the LDA+DMFT band structure no longer corresponds to an LDA band structure which is simply renormalized by a constant factor. Namely, the frequency dependence of the self-energy shows that the Fermi liquid regime strictly extends only from −0.2 eV to 0.15 eV. In this low-energy regime, the effective mass is somewhat higher ($m^\star_{\text{low}E}/m\approx 3$). Beyond this strict Fermi liquid regime the imaginary part of the self-energy stays relatively small, while the real part develops a shoulder. This shoulder translates into a kink in the effective quasiparticle dispersion, where the effective mass crosses over from $m^\star_{\text{low}E}$ to $m^\star$.

We carefully analyzed these features to make sure that they are not due to errors of QMC, MEM, or the inversion of the Dyson equation to determine the self-energy. Our findings, as well as the observation of similar features in numerical renormalization group calculations, prove that kinks in the effective band structure may originate from purely electronic correlations, i.e., without the presence of phonons, at least within the DMFT. In the mean time such kinks have been observed by Yoshida *et al.*[49] in the ARPES spectra of $SrVO_3$, albeit at energies somewhat closer to the Fermi level than predicted by our calculations. The microscopic preconditions for the existence of kinks reported in this paper are currently under detailed investigation.

ACKNOWLEDGMENTS

We thank J. W. Allen, J. Fink, P. Fulde, D. Manske, K. Matho, and Y.-F. Yang for helpful discussions. This work was supported by Russian Basic Research Foundation Grants No. RFFI-GFEN-03-02-39024_a (V.A.,I.N.,D.K.), No. RFFI-04-02-16096 (V.A.,I.N.,D.K.), No. RFFI-05-02-17244 (I.N.), No. RFFI-05-02-16301 (I.N.) and the Deutsche Forschungsgemeinschaft through Sonderforschungsbereich 484 (D.V.,G.K.,M.K.,I.N.), 436 RUS 113/723/0-1 (I.N.), the Emmy-Noether program (K.H.), and in part by the joint UrO-SO project N22 (V.A.,I.N.) programs of the Presidium of the Russian Academy of Sciences (RAS) "Quantum macrophysics" and of the Division of Physical Sciences of the RAS "Strongly correlated electrons in semiconductors, metals, superconductors, and magnetic materials." One of us (I.N.) acknowledges Dynasty Foundation and International Center for Fundamental Physics in Moscow program for young scientists 2005, Russian Science Support Foundation program for young PhD of Russian Academy of Science 2005 and grant of President of Russia for young PhD MK-2118.02.05.

[1] R. O. Jones and O. Gunnarsson, Rev. Mod. Phys. **61**, 689 (1989).
[2] V. I. Anisimov, A. I. Poteryaev, M. A. Korotin, A. O. Anokhin, and G. Kotliar, J. Phys.: Condens. Matter **9**, 7359 (1997); A. I. Lichtenstein and M. I. Katsnelson, Phys. Rev. B **57**, 6884 (1998).
[3] K. Held, I. A. Nekrasov, N. Blümer, V. I. Anisimov, and D. Vollhardt, Int. J. Mod. Phys. B **15**, 2611 (2001).
[4] K. Held, I. A. Nekrasov, G. Keller, V. Eyert, N. Blümer, A. K. McMahan, R. T. Scalettar, Th. Pruschke, V. I. Anisimov, and D. Vollhardt, Psi-k Newsletter **56**, 65 (2003), http://psi-k.dl.ac.uk/newsletters/News_56/Highlight_56.pdf.
[5] A. I. Lichtenstein, M. I. Katsnelson, G. Kotliar, in *Electron Correlations and Materials Properties*, 2nd ed., edited by A. Gonis, Nicholis Kioussis, and Mikael Ciftan (Kluwer Academic/Plenum, New York, 2002), p. 428.
[6] G. Kotliar and D. Vollhardt, Phys. Today **57**(3), 53 (2004).
[7] G. Kotliar, S. Y. Savrasov, K. Haule, V. S. Oudovenko, O. Parcollet, C. A. Marianetti, cond-mat/0511085 (unpublished).
[8] W. Metzner and D. Vollhardt, Phys. Rev. Lett. **62**, 324 (1989).
[9] D. Vollhardt, in *Correlated Electron Systems*, edited by V. J. Emery (World Scientific, Singapore, 1993), p. 57.
[10] Th. Pruschke, M. Jarrell, and J. K. Freericks, Adv. Phys. **44**, 187 (1995).
[11] A. Georges, G. Kotliar, W. Krauth, and M. J. Rozenberg, Rev. Mod. Phys. **68**, 13 (1996).
[12] I. A. Nekrasov, K. Held, N. Blümer, A. I. Poteryaev, V. I. Anisimov, and D. Vollhardt, Eur. Phys. J. B **18**, 55 (2000).
[13] K. Held, G. Keller, V. Eyert, D. Vollhardt, and V. I. Anisimov, Phys. Rev. Lett. **86**, 5345 (2001); S.-K. Mo, H.-D. Kim, J. W. Allen, G.-H. Gweon, J. D. Denlinger, J.-H. Park, A. Sekiyama, A. Yamasaki, S. Suga, P. Metcalf, and K. Held, *ibid.* **93**, 076404 (2004); G. Keller, K. Held, V. Eyert, D. Vollhardt, and V. I. Anisimov, Phys. Rev. B **70**, 205116 (2004).
[14] M. S. Laad, L. Craco, and E. Müller-Hartmann, Phys. Rev. Lett. **91**, 156402 (2003).
[15] V. I. Anisimov, D. E. Kondakov, A. V. Kozhevnikov, I. A. Nekrasov, Z. V. Pchelkina, J. W. Allen, S.-K. Mo, H.-D. Kim, P. Metcalf, S. Suga, A. Sekiyama, G. Keller, I. Leonov, X. Ren, and D. Vollhardt, Phys. Rev. B **71**, 125119 (2005).
[16] I. V. Solovyev, cond-mat/0506632 (unpublished).
[17] A. Liebsch, Phys. Rev. Lett. **90**, 096401 (2003).
[18] I. A. Nekrasov, G. Keller, D. E. Kondakov, A. V. Kozhevnikov, Th. Pruschke, K. Held, D. Vollhardt, and V. I. Anisimov, cond-mat/0211508 (unpublished), superceded by Ref. 20.
[19] E. Pavarini, S. Biermann, A. Poteryaev, A. I. Lichtenstein, A. Georges, and O. K. Andersen, Phys. Rev. Lett. **92**, 176403 (2004).
[20] A. Sekiyama, H. Fujiwara, S. Imada, S. Suga, H. Eisaki, S. I. Uchida, K. Takegahara, H. Harima, Y. Saitoh, I. A. Nekrasov, G. Keller, D. E. Kondakov, A. V. Kozhevnikov, Th. Pruschke, K. Held, D. Vollhardt, and V. I. Anisimov, Phys. Rev. Lett. **93**, 156402 (2004).
[21] I. A. Nekrasov, G. Keller, D. E. Kondakov, A. V. Kozhevnikov, Th. Pruschke, K. Held, D. Vollhardt, and V. I. Anisimov, Phys. Rev. B **72**, 155106 (2005).
[22] E. Pavarini, A. Yamasaki, J. Nuss, and O. K. Andersen, New J. Phys. **7**, 188 (2005).
[23] I. A. Nekrasov, Z. V. Pchelkina, G. Keller, Th. Pruschke, K. Held, A. Krimmel, D. Vollhardt, and V. I. Anisimov, Phys. Rev. B **67**, 085111 (2003).
[24] A. Liebsch and A. Lichtenstein, Phys. Rev. Lett. **84**, 1591 (2000).
[25] V. I. Anisimov, I. A. Nekrasov, D. E. Kondakov, T. M. Rice, and M. Sigrist, Eur. Phys. J. B **25**, 191 (2002).
[26] L. Craco, M. S. Laad, and E. Müller-Hartmann, Phys. Rev. Lett. **90**, 237203 (2003).
[27] A. I. Lichtenstein, M. I. Katsnelson, and G. Kotliar, Phys. Rev. Lett. **87**, 067205 (2001).
[28] S. Y. Savrasov, G. Kotliar, and E. Abrahams, Nature (London) **410**, 793 (2001).
[29] S. Y. Savrasov and G. Kotliar, Phys. Rev. B **69**, 245101 (2004).
[30] M. B. Zölfl, I. A. Nekrasov, Th. Pruschke, V. I. Anisimov, and J. Keller, Phys. Rev. Lett. **87**, 276403 (2001).
[31] K. Held, A. K. McMahan, and R. T. Scalettar, Phys. Rev. Lett. **87**, 276404 (2001).
[32] A. K. McMahan, K. Held, and R. T. Scalettar, Phys. Rev. B **67**, 075108 (2003).
[33] K. Haule, V. Oudovenko, S. Y. Savrasov, and G. Kotliar, Phys. Rev. Lett. **94**, 036401 (2005).
[34] A. K. McMahan, Phys. Rev. B **72**, 115125 (2005).
[35] B. Amadon, S. Biermann, A. Georges, and F. Aryasetiawan, cond-mat/0504732 (unpublished).
[36] A. K. McMahan, R. M. Martin, and S. Satpathy, Phys. Rev. B **38**, 6650 (1988).
[37] M. S. Hybertsen, M. Schlüter, and N. E. Christensen, Phys. Rev. B **39**, 9028 (1989).
[38] M. L. Knotek and P. J. Feibelman, Phys. Rev. Lett. **40**, 964 (1978).
[39] O. K. Andersen and T. Saha-Dasgupta, Phys. Rev. B **62**, R16219

(2000); O. K. Andersen, T. Saha-Dasgupta, S. Ezhov, T. Tsetseris, O. Jepsen, R. W. Tank, C. Arcangeli, and G. Krier, Psi-k Newsletter **45**, 86 (2001); O. K. Andersen, T. Saha-Dasgupta, and S. Ezhov, Bull. Mater. Sci. **26**, 19 (2003).

[40] A. Fujimori, I. Hase, H. Namatame, Y. Fujishima, Y. Tokura, H. Eisaki, S. Uchida, K. Takegahara, and F. M. F. de Groot, Phys. Rev. Lett. **69**, 1796 (1992).

[41] K. Maiti, D. D. Sarma, M. J. Rozenberg, I. H. Inoue, H. Makino, O. Goto, M. Pedio, and R. Cimino, Europhys. Lett. **55**, 246 (2001).

[42] A. Sekiyama, H. Fujiwara, S. Imada, S. Suga, H. Eisaki, S. I. Uchida, K. Takegahara, H. Harima, and Y. Saitoh, cond-mat/0206471 (unpublished), superceded by Ref. 20.

[43] I. H. Inoue, I. Hase, Y. Aiura, A. Fujimori, K. Morikawa, T. Mizokawa, Y. Haruyama, T. Maruyama, and Y. Nishihara, Physica C **235-240**, 1007 (1994).

[44] K. Morikawa, T. Mizokawa, K. Kobayashi, A. Fujimori, H. Eisaki, S. Uchida, F. Iga, and Y. Nishihara, Phys. Rev. B **52**, 13711 (1995).

[45] Y. Aiura, F. Iga, Y. Nishihara, H. Ohnuki, and H. Kato, Phys. Rev. B **47**, 6732 (1993); I. H. Inoue, I. Hase, Y. Aiura, A. Fujimori, Y. Haruyama, T. Maruyama, and Y. Nishihara, Phys. Rev. Lett. **74**, 2539 (1995); I. H. Inoue, O. Goto, H. Makino, N. E. Hussey, and M. Ishikawa, Phys. Rev. B **58**, 4372 (1998).

[46] M. J. Rozenberg, I. H. Inoue, H. Makino, F. Iga, and Y. Nishihara, Phys. Rev. Lett. **76**, 4781 (1996).

[47] H. Makino, I. H. Inoue, M. J. Rozenberg, I. Hase, Y. Aiura, and S. Onari, Phys. Rev. B **58**, 4384 (1998).

[48] R. Eguchi, T. Kiss, S. Tsuda, T. Shimojima, T. Yokoya, A. Chainani, S. Shin, I. H. Inoue, T. Togashi, S. Watanabe, C. Q. Zhang, C. T. Chen, M. Arita, K. Shimada, H. Namatame, and M. Taniguchi, Phys. Rev. Lett. **96**, 076402 (2006).

[49] T. Yoshida, K. Tanaka, H. Yagi, A. Ino, H. Eisaki, A. Fujimori, and Z.-X. Shen, Phys. Rev. Lett. **95**, 146404 (2005); A. Fujimori (private communication).

[50] M. J. Rey, P. H. Dehaudt, J. C. Joubert, B. Lambert-Andron, M. Cyrot, and F. Cyrot-Lackmann, J. Solid State Chem. **86**, 101 (1990).

[51] O. K. Andersen and O. Jepsen, Phys. Rev. Lett. **53**, 2571 (1984); The Stuttgart TB-LMTO-ASA Program, http://www.fkf.mpg.de/andersen/LMTODOC/LMTODOC.html.

[52] Our results are in agreement with LDA calculations within the LMTO-ASA method by S. Itoh, Solid State Commun. **88**, 525 (1993), and those by J. Takegahara, J. Electron Spectrosc. Relat. Phenom. **66**, 303 (1995) in the basis of augmented plane waves (APW). For our purposes, i.e., for the combination of the LDA band structure with DMFT,[2] the atomiclike wave functions basis set of the MTO method is however more appropriate.

[53] Ph. Lambin and J. P. Vigneron, Phys. Rev. B **29**, 3430 (1984); O. Jepsen and O. K. Andersen, Solid State Commun. **9**, 1763 (1971); P. E. Blöchl, O. Jepsen, and O. K. Andersen, Phys. Rev. B **49**, 16223 (1994).

[54] M. B. Zölfl, Th. Pruschke, J. Keller, A. I. Poteryaev, I. A. Nekrasov, and V. I. Anisimov, Phys. Rev. B **61**, 12810 (2000).

[55] O. Gunnarsson, O. K. Andersen, O. Jepsen, and J. Zaanen, Phys. Rev. B **39**, 1708 (1989).

[56] J. E. Hirsch and R. M. Fye, Phys. Rev. Lett. **56**, 2521 (1986). For multiband QMC within DMFT see Ref. 3.

[57] For a review of the maximum entropy method see M. Jarrell and J. E. Gubernatis, Phys. Rep. **269**, 133 (1996). In this work Sandvik's MEM code was used.

[58] S. Biermann, A. Dallmeyer, C. Carbone, W. Eberhardt, C. Pampuch, O. Rader, M. I. Katsnelson, and A. I. Lichtenstein, JETP Lett. **80**, 612 (2005).

[59] Th. A. Maier, Th. Pruschke, and M. Jarrell, Phys. Rev. B **66**, 075102 (2002).

[60] For a review of DCA see Th. Maier, M. Jarrell, Th. Pruschke, and M. H. Hettler, Rev. Mod. Phys. **77**, 1027 (2005).

[61] M. V. Sadovskii, I. A. Nekrasov, E. Z. Kuchinskii, Th. Pruschke, and V. I. Anisimov, Phys. Rev. B **72**, 155105 (2005); E. Z. Kuchinskii, I. A. Nekrasov, and M. V. Sadovskii, JETP Lett. **82**, 198 (2005).

[62] N. Blümer, Ph.D. thesis, Universität Augsburg, 2002.

[63] We thank J. Fink for useful discussions regarding these kinks during the 8th Japanese-German Symposium on Competing Phases in Novel Condensed Matter Systems, Lauterbad, August 2004, where our results were first presented. We also thank him and P. Fulde for useful discussions at the International Workshop on Strong Correlations and ARPES: Recent Progress in Theory and Experiment, Max-Planck Institute for Physics of Complex Systems, Dresden, April 2005.

[64] G. Keller, D. E. Kondakov, I. Nekrasov, K. Held, T. Pruschke, V. I. Anisimov, and D. Vollhardt, International Conference on Strongly Correlated Electron Systems SCES '04, Abstract Booklet WE-TMO3-55, p. 131; G. Keller, V. I. Anisimov, D. E. Kondakov, A. V. Kozhevnikov, I. A. Nekrasov, Z. V. Pchelkina, I. Leonov, X. Ren, and D. Vollhardt, Verh. Dtsch. Phys. Ges. **40**, 2/2005, TT 16.87, p. 580.

[65] A. Lanzara, P. V. Bogdanov, X. J. Zhou, S. A. Kellar, D. L. Feng, E. D. Lu, T. Yoshida, H. Eisaki, A. Fujimori, K. Kishio, J.-I. Shimoyama, T. Noda, S. Uchida, Z. Hussain, and Z.-X. Shen, Nature (London) **412**, 510 (2001). For reviews see T. Cuk, D. H. Lu, X. J. Zhou, Z.-X. Shen, T. P. Deveraux, and N. Nagaosa, Phys. Status Solidi B **242**, 11 (2005); A. Damascelli, Z. Hussain, and Z.-X. Shen, Rev. Mod. Phys. **75**, 473 (2003).

[66] D. Manske, I. Eremin, and K. H. Bennemann, Phys. Rev. Lett. **87**, 177005 (2001); Phys. Rev. B **67**, 134520 (2003).

[67] Y. Kakehashi and P. Fulde, J. Phys. Soc. Jpn. **74**, 2397 (2005).